

# Can the temperature of a freezing liquid increase?

Virkeshwar Kumar, Atul Srivastava, Shyamprasad Karagadde\*

Department of Mechanical Engineering, Indian Institute of Technology Bombay, Mumbai  
400076, India

\* Corresponding author: email address – s.karagadde@iitb.ac.in

## Abstract

In this study, identical experiments of bottom-cooled solidification of water-23 wt%  $\text{KNO}_3$  and water-24 wt%  $\text{NH}_4\text{Cl}$ , which exhibit faceted and dendritic microstructures respectively, were performed. The primary objective of this investigation is to understand the role of solidification morphology (mushy zone) and the flow characteristics on the temperature of the bulk fluid. The strength of compositional convection was correlated with the help of Rayleigh number in both mushy and bulk-fluid zones and was further used to assess the flow behaviour during faceted and dendritic growths. Based on the liquid temperature profile during faceted growth, three distinct regimes of heat transfer were observed in the liquid, namely - *convection-dominated*, *transition*, and *conduction-dominated*. The experimental findings revealed an anomalous temperature rise of the bulk liquid when the mushy-zone permeability was restricted by the faceted grain morphology. The observed temperature rise was further ascertained with the help of energy balance in an indicative control volume ahead of the interface, and the role of natural convection patterns in controlling the local freezing and thermal distribution. Moreover, the results clearly showed that the existence of a suitable length-scale of the freezing front, such as the primary arm spacing, cannot always lead to plume formation.

## 1. Introduction

Natural convection in liquid during solidification can considerably affect the composition and temperature distribution, which in turn alters the growth of the solid in the mushy zone [1]. The buoyant forces due to the rejection of less-dense residual liquid in the mushy zone (e.g., the bottom cooling of the hyper-eutectic water-salt systems) resist the frictional forces [2,3]. The formation of the plumes, which are also termed as solute channels, or chimney [4–6], is known to occur when the strength of the buoyant force exceeds a minimum threshold [3,6]. Likewise, the stabilization of convection in the form of plumes is typically characterized by a critical Rayleigh number in the mushy zone. Worster [7] formulated a permeability-based Rayleigh number in the mushy zone using two different types of length scales, i.e., (a) height of the mushy zone and (b) the ratio of

thermal diffusivity to the growth rate [7,8]. Ramirez and Beckerman [9] reported a combined study for the formation of plumes in Pb-Sn and Ni-base superalloys, with the average permeability estimated using both Blake-Kozeny and Poirier's relations and the two prior mentioned length scales. Yuan and Lee [5] stated that the competition between upward solute transport and dendritic growth determined the survival of the plumes.

The solidifying interface can be classified as either diffuse or faceted, where the formation of the latter is primarily attributed to a higher entropy of phase change at the melting temperature [10]. Dendritic morphology is a diffuse interface which is mostly found in metallic systems and a few transparent materials such as succinonitrile, camphor,  $\text{NH}_4\text{Cl}$ ,  $\text{Na}_2\text{ClO}_3$ , etc [4,11–13]. The faceted growth is generally observed in semiconductors, oxides, carbides, and complex non-metallic compounds such as  $\text{KNO}_3$ ,  $\text{CuSO}_4$ ,  $\text{Na}_2\text{SO}_4$  [10,12,14–18]. The microstructural morphology together with the solid fraction (equivalent to a packing fraction in a porous medium) considerably affects the transport of rejected component, particularly when it is lighter compared to the bulk fluid density. A number of studies have reported convection and temperature measurements in the liquid during bottom cooled solidification of hyper-eutectic water- $\text{NH}_4\text{Cl}$  system [19,20], in which the primary convection is compositionally driven, in the presence of a positive thermal gradient in the vertical direction. However, contrasting flow and thermal behaviors have been reported when the primary solid is in the faceted form. Vigorous convective flow was observed during the solidification of water- $\text{Na}_2\text{SO}_4$ , and water- $\text{CuSO}_4$  [11,14,18], under side and top cooled conditions. Thompson et al. [21] performed bottom-cooled experiments involving  $\text{KNO}_3$  as one of the constituents, and reported vigorous and random convection for a certain duration where  $\text{KNO}_3$  was the primary solidifying component. Further, a gain in the bulk fluid temperature was also observed at the end of convection in [21], which was attributed to heat gained from the surroundings. This may not be necessarily true, as the distinguishing flow patterns with dendritic and faceted morphologies control the heat and mass transfer within the liquid.

In order to understand the mechanisms of flow under the said two morphological conditions, and to assess the uncharacteristic temperature rise, we performed real-time observations of bottom-cooled solidification of water- $\text{NH}_4\text{Cl}$  and water- $\text{KNO}_3$  mixtures, with measurement of temperature from several locations along of the height of the solidification cell. The density-based shadowgraph technique and particle image velocimetry (PIV) were employed for performing the qualitative and

quantitative flow characterization respectively. Two different Rayleigh numbers, based on the bulk fluid and mushy zone volumes were evaluated to measure the convective strength in the respective zones. The temperature rise during the faceted growth has been quantified, and a plausible hypothesis for the anomalous temperature behaviour is proposed.

## 2. Experimental setup and procedure

### 2.1 Materials

Water-KNO<sub>3</sub> and water-NH<sub>4</sub>Cl aqueous binary solutions were used to obtain faceted and dendritic morphology of the primary  $\beta$ -solid respectively. The density of water, NH<sub>4</sub>Cl, and KNO<sub>3</sub> are 1, 1.57 and 2.11g/cm<sup>3</sup> respectively. Eutectic temperatures of binary eutectic systems, water-9 wt% KNO<sub>3</sub> and water-19.7 wt% NH<sub>4</sub>Cl, are -2.84 °C and -13.9 °C, respectively [22,23]. At these compositions, the expected solid fraction values at the eutectic temperature are 0.17 and 0.07. In the present study, the hyper-eutectic regime was chosen to perform experiments where a low-density mixture was rejected at the solidifying interface. Water-23 wt% KNO<sub>3</sub> and water-24 wt% NH<sub>4</sub>Cl were the initial compositions, and their corresponding liquidus temperatures were 18 °C, and 6 °C respectively [22,24]. The details of thermo-physical properties are listed in Table 1.

Table 1: Thermo-physical properties of water-KNO<sub>3</sub> and water-NH<sub>4</sub>Cl systems [21,22,24–26]

Parameters (Units)	Symbol	water-KNO <sub>3</sub>	water-NH <sub>4</sub> Cl
Initial composition (wt %)	$C_o$	23	24
Eutectic composition (wt %)	$C_E$	9	19.7
Eutectic Temperature (°C)	$T_E$	-2.84	-13.91
Liquidus Temperature (°C), (C wt% of KNO <sub>3</sub> or NH <sub>4</sub> Cl)	$T_l$	1.5C-16.305	4.61C-104.6
Thermal diffusivity ( $m^2/s$ )	$\alpha$	$1.33 \times 10^{-7}$	$1.5 \times 10^{-7}$
Solutal diffusivity ( $m^2/s$ )	$D$	$2.23 \times 10^{-9}$	$2.2 \times 10^{-9}$
Thermal conductivity of liquid ( $W/m.k$ )	$k_l$	0.52	0.468
Thermal conductivity of solid ( $W/m.k$ )	$k_s$	2.6	2.7
Solutal expansion coefficient ( $wt \%^{-1}$ )	$\beta_C$	$6.04 \times 10^{-3}$	$2.57 \times 10^{-3}$
Kinematic viscosity ( $m^2/s$ )	$\nu$	$1.21 \times 10^{-6}$	$1.21 \times 10^{-6}$
Density of liquid ( $Kg/m^3$ ) at $T_E$	$\rho_l$	1063	1055
Density of solid ( $Kg/m^3$ )	$\rho_s$	1527	1527
Latent heat of fusion ( $KJ/Kg$ )	$H$	496	313

## 2.2 Experimental setup, instrumentation and measurements

The bottom-cooled solidification cell was made of 8 mm thick perspex glass, as shown in Figure 1. The inner volumetric dimension of the cell was  $110 \times 70 \times 50 \text{ mm}^3$ . To prevent the condensation problem during *in situ* experiments, a cover cell was placed on the solidification cell. The bottom copper plate of the cell was maintained at  $-22^\circ\text{C}$  using an assembly of peltier, TEC controller, DC power supply, heat exchanger, and a julabo circulating bath [20,27]. Nine *K*-type thermocouples (accuracy of  $\pm 0.15^\circ\text{C}$ ) were attached to each of the vertical sidewalls to measure the temperature. The temperature data was acquired through data loggers (PICO ® TC-08).

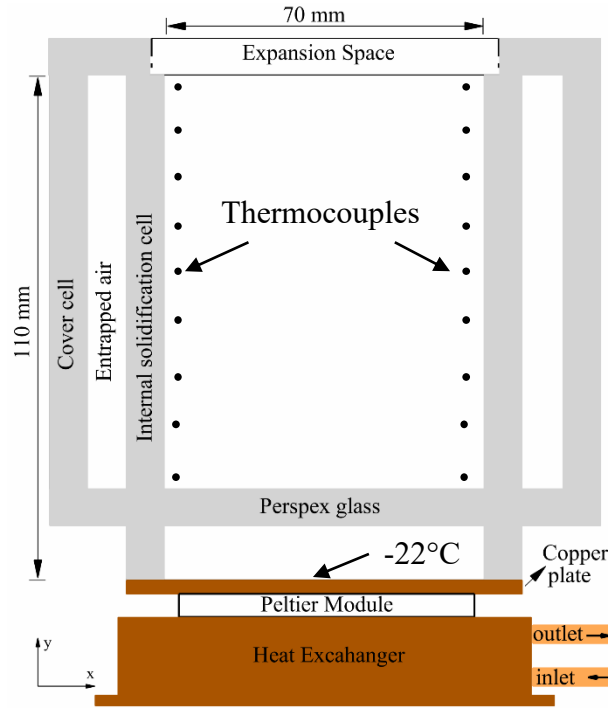


Figure 1: Schematic of solidification cell.

The density is known to be a function of temperature and composition. For observing the buoyant convection patterns during the experiments, the density gradient based shadowgraph technique was employed. In shadowgraph, a white light source (250 W) was collimated using a plano-convex lens. The collimated beam was passed through the solidification cell, and density changes in the cell were captured by a CCD camera (Imperx CLB-B2520M). For the velocity measurements of liquid, particle image velocimetry (MicroVec PIV ®) was employed. PIV system consists of a DPSS laser (532 nm), synchronizer, and a CCD camera (Imperx CLB-B2520M, resolution 2456

× 2048). Neutrally buoyant hollow glass particles (average diameter 10 μm) were used as seeding particles. The details of the employed PIV setup can be found in the references [28,29].

The calibration curve of the refractive index with known composition was established using a refractometer (Anton Paar ®). Samples were extracted from the cell during the experiment, and the refractive index was measured. Using the calibration curve and measured refractive index of samples, the composition of KNO<sub>3</sub> and NH<sub>4</sub>Cl was evaluated.

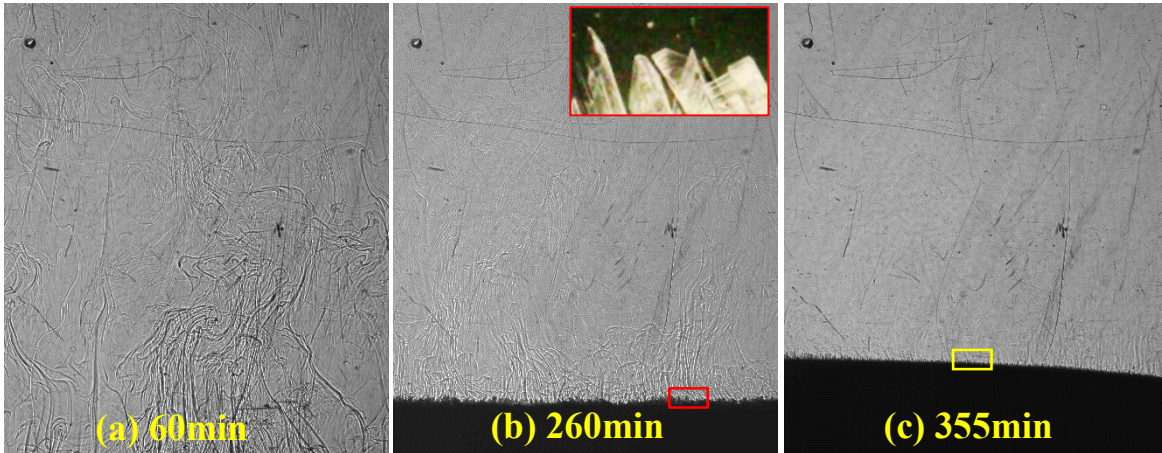
### 3. Observations

#### 3.1 Convective flows in faceted and dendritic growth cases

Figure 2 shows the spatio-temporal evolution of the flow field obtained from the shadowgraphs during the bottom cooled solidification of water-23 wt% KNO<sub>3</sub> (a-c), and water-24 wt% NH<sub>4</sub>Cl (d-f). In water-23 wt% KNO<sub>3</sub>, the flow of rejected (low dense) mixture was random (not in specific patterns such as plume, Figure 2(a)), whereas in water-24 wt% NH<sub>4</sub>Cl, the plume formation and localized solutal convection (near bottom section) were observed (Figure 2(d)). Evolving microstructures were captured using a portable microscope (Dinolite ®, Model AM7515MZT). The faceted and dendritic solid was observed in water-23 wt% KNO<sub>3</sub> (inset of Figure 2(b)), water-24 wt% NH<sub>4</sub>Cl (inset of Figure 2(e)) respectively.

The random convective flow essentially homogenized the composition and temperature of the liquid in the cell (particularly ahead of the mushy zone), and reduced the bulk composition to near eutectic composition within 300 min. Note that in Figure 2(c), the macroscopic freezing interface is slightly inclined, which could be attributed to slight variations in the compositional distribution induced by the random convective flow patterns. The composition of the bulk fluid and the strength of convection were found to further reduce with time, which was measured to be water-11.8 wt % KNO<sub>3</sub> at 350 min. At 600 min, the composition reached the uniform eutectic composition water-9.9±.3 wt% KNO<sub>3</sub>, and interface became flat (Figure 3(a-c)) from previous time instants (Figure 2(c)).

### Faceted growth (water-KNO<sub>3</sub>)



### Dendritic growth (water-NH<sub>4</sub>Cl)

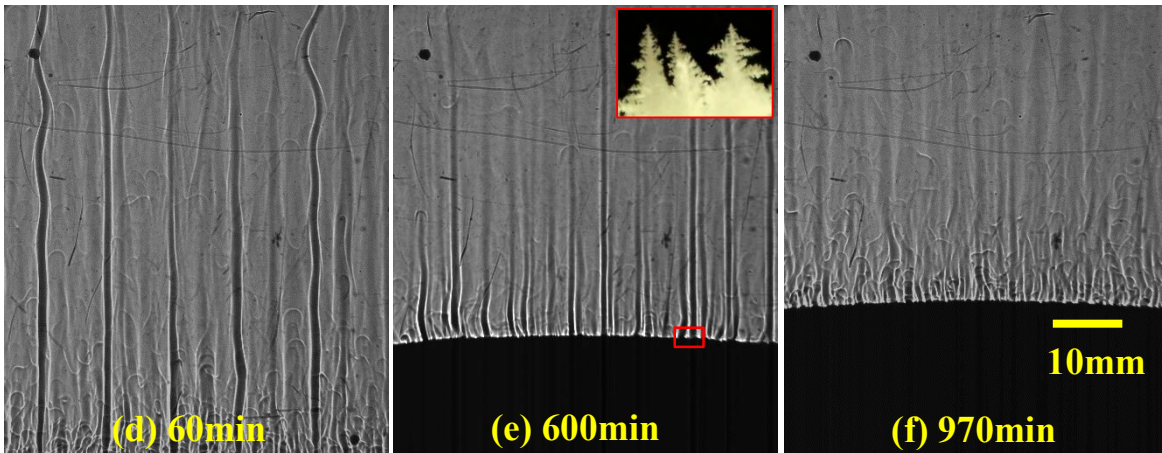
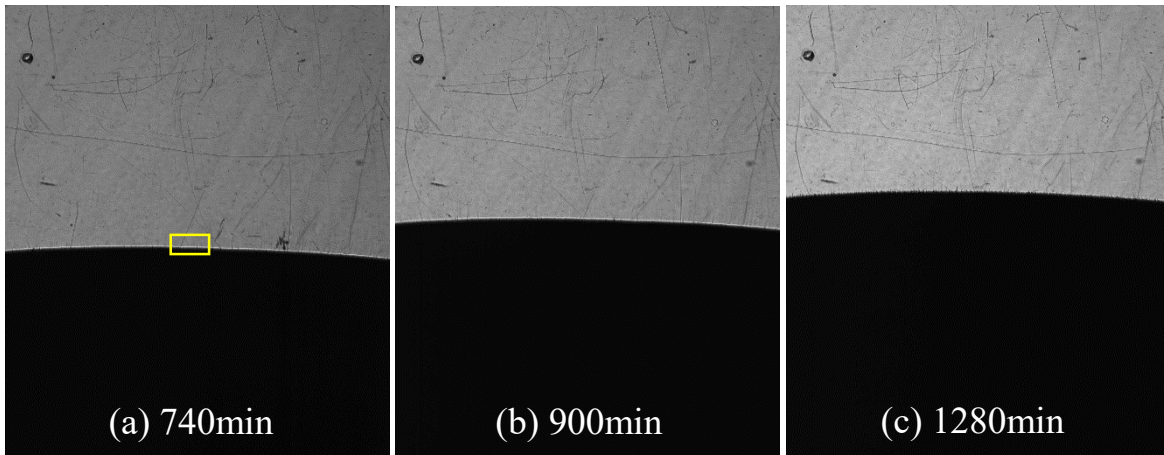


Figure 2: Convective flow observation using shadowgraph (a-c) for water-23 wt% KNO<sub>3</sub>: (a) random solutal convection at 60 min (b) similar flow at 260 min, and faceted microstructure was shown in the inset of figure, (c) the composition reached near eutectic composition and the sloped interface was observed at 355 min, and (d-f) for water-24 wt% NH<sub>4</sub>Cl (d) plume formation at 60 min (e) dendritic morphology captured at solid-liquid interface presented in the inset of figure at 600 min (f) localized solutal convection at 970 min. (Note: The yellow rectangular box on the interface in (c) used for intensity measurements).

In the case of dendritic growth, the solutal convection dominated in the form of plumes which developed a solutal gradient in the direction of gravity. Hence, it would take a much longer time to reach the eutectic composition. At 600 min, the compositions at the top of the cell and near the solidifying interface were water-21.3 wt% NH<sub>4</sub>Cl and water-22.47 wt% NH<sub>4</sub>Cl respectively. The growth was comparatively slower between 970 min (Figure 2(f)) to 1410 min (Figure 3(d)) due to continuous change in composition and the liquidus temperature. Composition reached closer to the eutectic composition (water-20.05 wt% NH<sub>4</sub>Cl) at 1410min. Furthermore, eutectic solid was observed much later, at 1410 min (Figure 3(e, f)), compared to 600 min in the faceted case.

### Faceted growth (water-KNO<sub>3</sub>)



### Dendritic growth (water-NH<sub>4</sub>Cl)

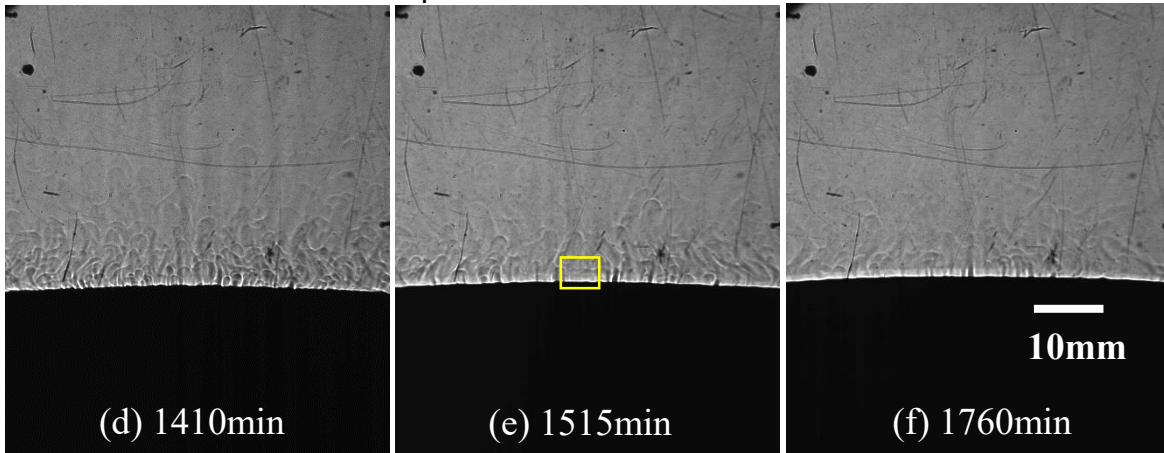


Figure 3: Eutectic growth was observed using shadowgraph (a-c) for water-23wt% KNO<sub>3</sub>: at (a) 740 min (b) 900 min (c) 1280 min and (d-f) for water-24wt% NH<sub>4</sub>Cl: (d) localized solutal convection occurs with composition reached near the eutectic composition at 1410 min (e) eutectic growth at 1515 min (f) similar eutectic growth at 1760 min. The yellow rectangular box on the interface in (a, d and e) used for intensity measurements.

### 3.2 Role of convection on the evolution of solid

In the two hyper-eutectic binary mixtures (water-23 wt% KNO<sub>3</sub> and water- 24 wt% NH<sub>4</sub>Cl), the primary solid ( $\beta$ ) phase is primarily the salt system. At temperatures below the eutectic line, the solid exists as a mixture of  $\beta$ -solid and the eutectic (existing in the inter-granular regions). In the present experiments, such a solid phase was observed at the bottom of the cell and is termed as  $\beta$ +eutectic solid (Figure 4 (a, b)). On comparing the solidifying structures of the two binary mixtures, the formation of a larger amount of eutectic solid in the faceted case was observed, as the liquid ahead of the freezing mixture was able to reach near-eutectic composition uniformly due

to stronger convective mixing (Figure 4(c)). In water-24 wt%  $\text{NH}_4\text{Cl}$ , the liquid composition was much slower in reaching near-eutectic composition, and therefore the pure eutectic solid was considerably lesser. Moreover, the rate of growth of the uppermost location of the freezing interface was found to be considerably larger in the eutectic growth for the faceted case.

The existence of a fully eutectic phase, and the mixture of primary and eutectic phases were ascertained by measuring the composition of the solid at the end of the experiments. The change in the mass of the solid sample was evaluated by evaporating the water from the solid mixture. In the faceted case, the average composition of  $\beta$ +eutectic and the eutectic was  $55\pm 3$  wt% and  $14\pm 1$  wt%  $\text{KNO}_3$  respectively, whereas in the dendritic case, the average composition of the  $\beta$ +eutectic solid was  $32\pm 2$  wt%  $\text{NH}_4\text{Cl}$ .

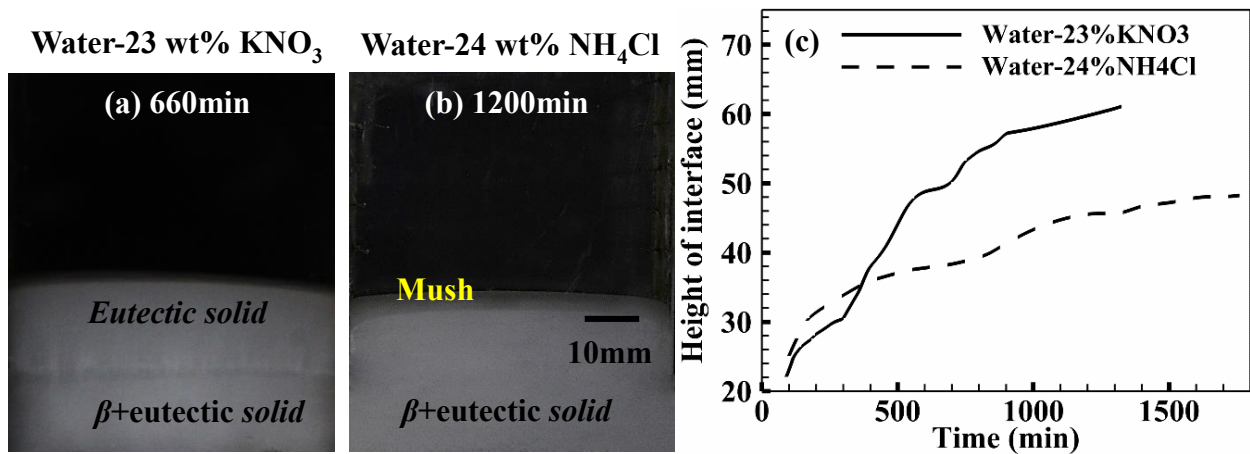


Figure 4: Evolution of solid (captured using Canon 1200D) during solidification of (a) water-23 wt%  $\text{KNO}_3$  at 660min (b) water-24 wt%  $\text{NH}_4\text{Cl}$  at 1200min. (c) Comparison of the height of interface with the time of experiments between water-23 wt%  $\text{KNO}_3$  and water-24 wt%  $\text{NH}_4\text{Cl}$ .

### 3.3 Velocity field in bulk fluid

In the faceted growth, the maximum velocity magnitude was 4.1 mm/sec at 100min (Figure 5(a)), and it reduced to 3.3 mm/sec (at 120min) with time (Figure 5(b)). As the solidification progressed, the convection strength decreased due to the shifting of composition towards the eutectic composition, which led to a decrease in velocity magnitude with time (Figure 5(a, b)).

After the initial solutal convection during dendritic growth, stabilized plumes were observed in the cell (Figure 5(c)). The approximate average velocity of plumes was 0.6 mm/s and that of the bulk

fluid was much lower ( $\sim 10^{-2}$  mm/s). However, in the faceted case, the velocity field in the bulk fluid was uniform but larger in magnitude (2-4 mm/s).

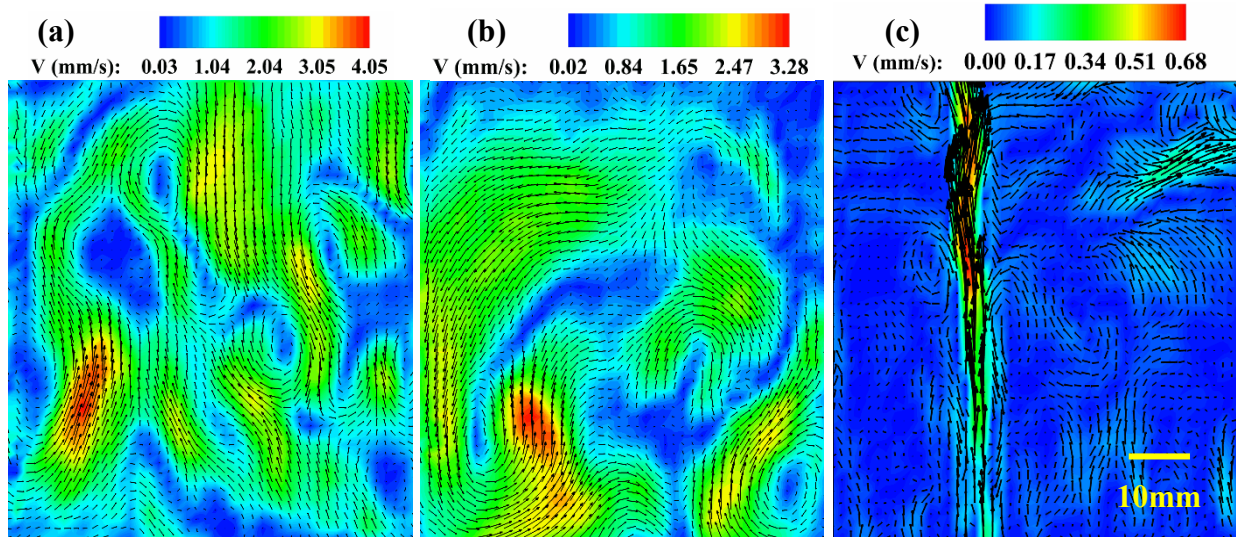


Figure 5: Velocity contours and vector in: faceted growth (water-23wt%  $\text{KNO}_3$ ) at (a) 100min (b) 120min where random and higher velocity magnitude was observed compared to (c) dendritic growth (water-23wt%  $\text{NH}_4\text{Cl}$ ) at 100min.

### 3.4 Uncharacteristic temperature rise in the faceted case

Figure 6 shows the temperature measurements at different locations along with height of the cell for the faceted (water-23 wt%  $\text{KNO}_3$ , Figure 6(a)) and dendritic (water-24 wt%  $\text{NH}_4\text{Cl}$ , Figure 6(b)) growth cases. Significantly dissimilar temperature profiles were observed for the two cases, with the faceted solidification showing drastic initial cooling, followed by an unusual temperature rise. On the contrary, the temperature profiles of the dendritic case showed slow but gradual temperature decrease, on par with the nominal cooling rate. Moreover, both the cases demonstrated a slight temperature rise towards the end of the experiment (marked by the gray box in Figure 6(a-b)), which is very likely to have been associated with the heat gained from the surroundings. Based on the changes in the slope of temperature vs time measurements of the faceted case, the following three modes of heat transfer in the liquid have been identified: (a) *convection-dominated regime*, (b) *transition regime* and (c) *conduction-dominated regime*. Note that similar regimes were identified in the dendritic case as well, but the changes in slopes were relatively less severe.

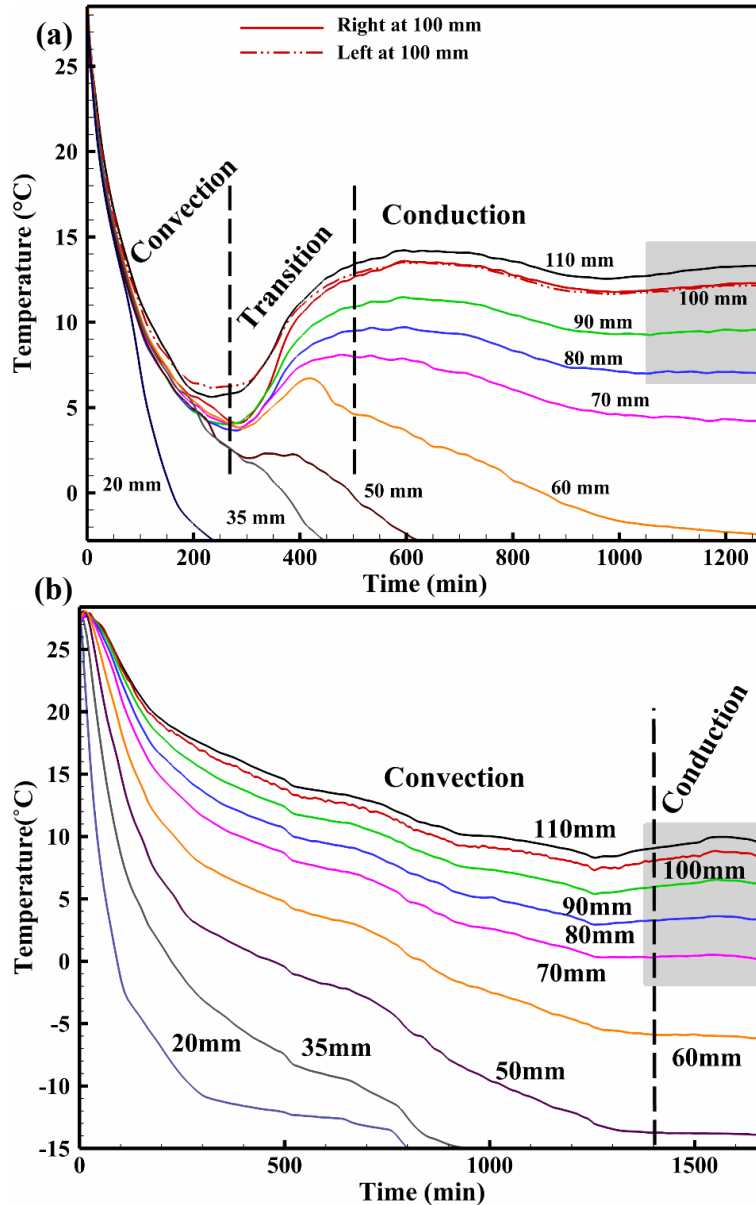


Figure 6: Temperature measurement at the different position in the cell for (a) higher cooling rate, gain in temperature and conduction dominated cooling in liquid was observed in solidification of water-23 wt% KNO<sub>3</sub> (b) slow cooling in liquid was observed in water-24 wt% NH<sub>4</sub>Cl

### 3.4.1 Convection-dominated regime

In the faceted case, vigorous and random convective flow decreased the temperature very rapidly and considerably low vertical thermal gradients were noticed at all the measurement locations (Figure 6(a)). This phase is termed as the *convection-dominated regime*. For the dendritic case, the

temperature of the fluid decreased with the nominal cooling rate (much lower than water-KNO<sub>3</sub> case) due to the presence of well-defined convective patterns (plumes), as shown in Figure 6(b).

### 3.4.2 Transition regime

At the end of the *convection dominated regime*, low thermal gradients were observed in the bulk fluid. The bulk fluid composition reached closer to the eutectic composition, where localized solutal convection, eutectic growth, and a gain in the temperature were observed. This region was termed as the *transition regime* (300min to 500min) (Figure 6(a)). Similar gain in the bulk liquid temperature was observed by Thompson et al. [21] during bottom cooled solidification of water-KNO<sub>3</sub>-NaNO<sub>3</sub> where KNO<sub>3</sub> was the primary solidifying component, however, the increase was attributed to change in the temperature of the surrounding environment. In the present work, we further observed gain in the temperature with different initial compositions of water-KNO<sub>3</sub> system. In order to verify the temperature rise in different faceted-forming mixtures, experiments with the hyper-eutectic mixtures of water-Na<sub>2</sub>SO<sub>4</sub> were performed, where similar random convection patterns and gain in temperatures were observed during bottom-cooled solidification (data in appendix). In the end of *transition regime*, the solid-liquid interface was flat and beyond this regime, the phenomenon was termed as *Conduction-dominated regime*.

In water-NH<sub>4</sub>Cl (dendritic growth) case, a positive thermal gradient in the liquid was available (Figure 6(b)). The gain in temperature, and hence transition regime did not exist unlike the case of water-KNO<sub>3</sub> (faceted growth).

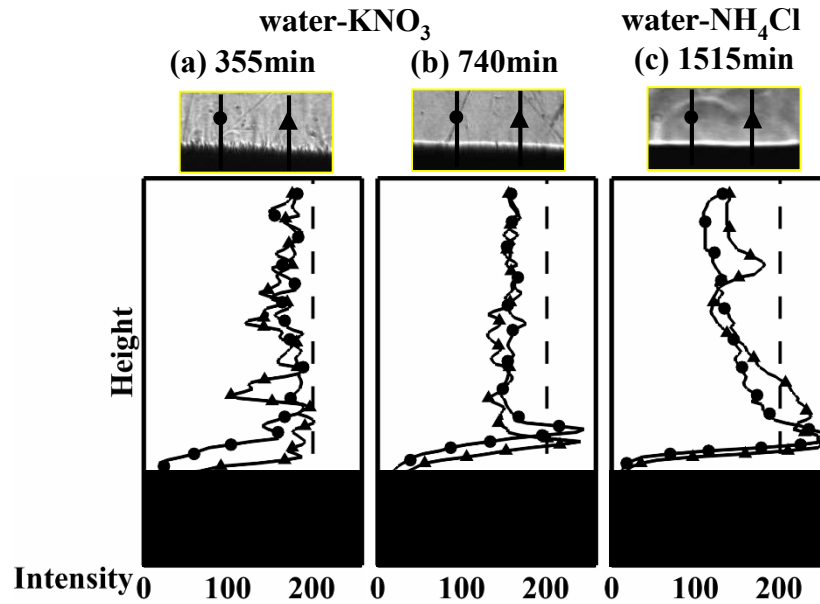
### 3.4.3 Conduction-dominated regime

In *conduction-dominated regime*, the temperature decreased gradually, with continuous growth of the eutectic solid. As a result, a larger thermal gradient in the liquid was set-up at the interface, which appeared to deflect the collimated light in the shadowgraphs by showing a high grayscale intensity. The intensity measurements at different locations near the solid-liquid interface (marked rectangular box in Figure 2 and 3) are shown in Figure 7. A high intensity (grayscale intensity

magnitude  $\sim 255$ ) uniform band was observed in Figure 7(b) at the interface (740 min), unlike Figure 7(a) when the localized convection was present at 355min.

Similarly, in water-NH<sub>4</sub>Cl (Figure 3(d-f)) case, the eutectic growth led to a high gradient region at the interface after 1410 min. From the temperature and the intensity measurements, the gradient near the interface was observed to be higher in water-NH<sub>4</sub>Cl (Figure 6(b), 7(c)) than the water-KNO<sub>3</sub> (Figure 6(a) and 7(b)) system.

Figure 7: Correlation of the temperature gradients along with the height at the solid-liquid interface with the help of gray-scale intensity variation; (a) convection-dominated regime and b)



conduction-dominated regime in water-23 wt% KNO<sub>3</sub>, (c) conduction-dominated regime in water-24 wt% NH<sub>4</sub>Cl.

## 4. Discussion

### 4.1 Analysis of flow behaviour using Rayleigh number

It is now clearly understood that the convective flow patterns in the bulk are strongly influenced by the mushy zone morphology. Based on two distinct volumetric zones of the flow, the following two cases were considered for the estimation of convective strength; (a) permeable or mushy zone fluid (b) bulk fluid.

#### 4.1.1 Flow through the permeable mushy zone

The strength of solutal convection in the mushy zone can be estimated using the permeability-based Rayleigh number ( $Ra_{c_p}$ ), which is formulated in Eq (1) [7,9].

$$Ra_{c_p} = \frac{g\beta_c\Delta C_p Kl}{D\nu} \quad (1)$$

where  $g$  is the gravitational acceleration,  $\beta_c$  is the solutal expansion coefficient,  $K$  is the average permeability,  $l$  is the length scale,  $D$  is the solutal diffusivity,  $\nu$  is the kinematic viscosity and  $\Delta C_p$  is the composition difference between the initial and inter-granular regions. All the thermo-physical properties were taken as constant and details are mentioned in (Table 1).  $Kl$  is the volumetric length scale in the mushy zone. For unidirectional solidification, the growth rate is not constant; hence the length scale ( $l$ ) was chosen to be the height of the mushy zone instead of the ratio of thermal diffusivity and growth rate. The permeability based Rayleigh number ( $Ra_{c_p}$ ) was calculated to be 68 and 231 for the water-KNO<sub>3</sub> and water-NH<sub>4</sub>Cl systems at 100 min respectively. Literature suggested that below the critical permeability-based Rayleigh number ( $Ra_{c_p}$ ), the plumes were suppressed. In the present study, critical  $Ra_{c_p}$  was estimated to be 115. The critical  $Ra_{c_p}$  was evaluated with the minimum composition difference required at the onset of plumes.

The average permeability ( $K = 6 \times 10^{-4} \lambda^2 \frac{(1-f_s)^3}{f_s^2}$ , Blake-Kozeny equation [9]) is a function of the primary arm spacing ( $\lambda$ ) and the mean solid fraction ( $f_s$ ) in the mushy zone. These parameters were estimated from the images of the microstructures, shown in the insets of Figures 2(b) (for water-KNO<sub>3</sub>) and 2(e) (for water-NH<sub>4</sub>Cl). In the faceted case, The higher solid fraction and primary arm spacing typically result in a low value of the permeability ( $K$ ) (Table 2), which, along with a lower mushy zone height ( $l$ ) leads to a low solutal Rayleigh number. In the present study it was observed, that the permeability-based Rayleigh number was lesser for faceted case than that

of the critical  $Ra_{c-p}$  (Table 2) and therefore, the condition for the formation of the plumes was not met (Figure 2(a, b)).

Table 2: Experimental details during solidification of water-23wt%  $KNO_3$  and water-24wt%  $NH_4Cl$

Parameters (Units)	Symbol	water- $KNO_3$	water- $NH_4Cl$
Fraction of solid in mushy zone	$f_s$	0.82	0.45
Primary arm spacing (mm)	$\lambda$	3	0.9
Mushy zone height (mm)	$l$	11	19
Average permeability at 100 min	$K$	$4.7 \times 10^{-11}$	$4.9 \times 10^{-10}$
Growth rate ( $\mu\text{m/s}$ ) at 100 min	$V$	1.8	1.3
Mushy zone length scale (m)	$\frac{\alpha}{V}$	0.08	0.1
Growth rate ( $\mu\text{m/s}$ )	$V$	1.55	0.58
		(300-500 min)	(1000-1400 min)

#### 4.1.1 Flow through the bulk fluid

The convective velocity scale in the bulk fluid ( $V_{scale} \approx \sqrt{g\beta_C\Delta Ch} \sim Ra_{c-Bulk}^{0.5} h^{-1}$ ) is proportional to the solutal expansion coefficient ( $\beta_C$ ),  $\Delta C$  (composition difference between the initial and the instantaneous bulk fluid compositions in water- $KNO_3$  system, and composition difference between the initial and the plume compositions in water- $NH_4Cl$  case) and  $h$  (height of liquid) or solutal  $Ra$  in bulk fluid ( $Ra_{c-Bulk}$ ). For estimating the bulk fluid velocities, a differently scaled  $Ra$  is necessary. The solutal Rayleigh number in bulk fluid ( $Ra_{c-Bulk}$ ) is defined with liquid height as length scale, and it is expressed as Eq. (2).

$$Ra_{c-Bulk} = \frac{g\beta_C\Delta Ch^3}{D\nu} \quad (2)$$

where  $h$  is the height of liquid and  $h^3$  being the volumetric length scale for bulk fluid. Higher values of  $\beta_C$ ,  $\Delta C$  and  $h$  (Figure 4(c)) led to higher solutal Rayleigh number in the faceted case (water- $KNO_3$ ). At 100 min, solutal Rayleigh number in the bulk fluid for water-23 wt %  $KNO_3$  was  $9.1 \times 10^9$  and  $1.7 \times 10^9$  for water-24 wt %  $NH_4Cl$ . Similarly, water- $KNO_3$  has higher velocity scale (7.5 mm/s at 100 min) than water- $NH_4Cl$  (2 mm/s at 100 min), which agreed well with the experimental data obtained from PIV (Figure 5). Figure 8 shows the transient variation of non-

dimensional solutal Rayleigh number in bulk fluid. Non-dimensional solutal Rayleigh number in bulk fluid is the ratio of instantaneous Rayleigh number to the maximum Rayleigh number. While the maximum solutal convection occurred at the same instant for both the cases, a lower mushy zone permeability of the faceted rapidly suppressed the convection.

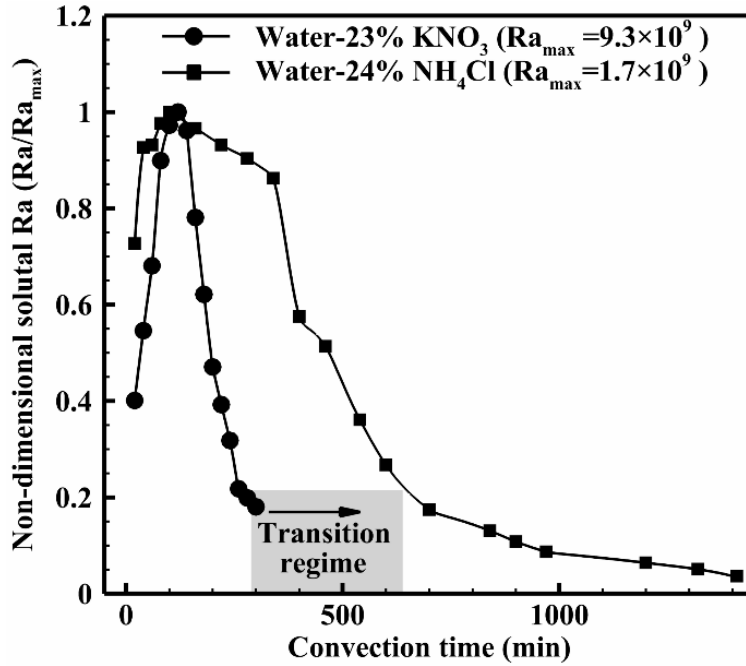


Figure 8: Non-dimensional solutal  $Ra$  ( $Ra/Ra_{max}$ ) in bulk fluid vs. time for the water-23wt%  $KNO_3$  and water-23wt%  $NH_4Cl$  experiments.

#### 4.2 Energy balance in the transition regime

In order to correlate the role of natural convection patterns to the anomalous rise of liquid temperature in the faceted case, energy balance for a control volume was analyzed by considering the solidification of a differential volume element  $dV$ . Figure 9(a) shows an image of the experiment (water- $KNO_3$ , time = 400 min) in which a representative control volume at the interface is considered (Figure 9(b)). The energy balance at the interface for the growth of  $dV$  amount of solid during the 300-500 min is expressed as Eq. (3)

$$k_s \frac{dT_s}{dx} - \rho_s H dV = \rho_l C_{pl} \Delta T_{change} V + k_l \frac{dT_l}{dx} \quad (3)$$

where  $\frac{dT}{dx}$  is the thermal gradient, with subscripts  $s$  and  $l$  corresponding to the solid and liquid sides of the control volume,  $k$  is the thermal conductivity,  $\rho$  is the density,  $H$  is the latent heat of fusion,  $V$  is the average growth rate during 300-500min,  $C_p$  is the specific heat of capacity,  $\Delta T_{change}$  is the change in temperature in liquid,  $\Delta t$  is the duration of time (300-500 min). Thermo-physical properties and experimental details for present study are shown in Table 1 and Table 2.

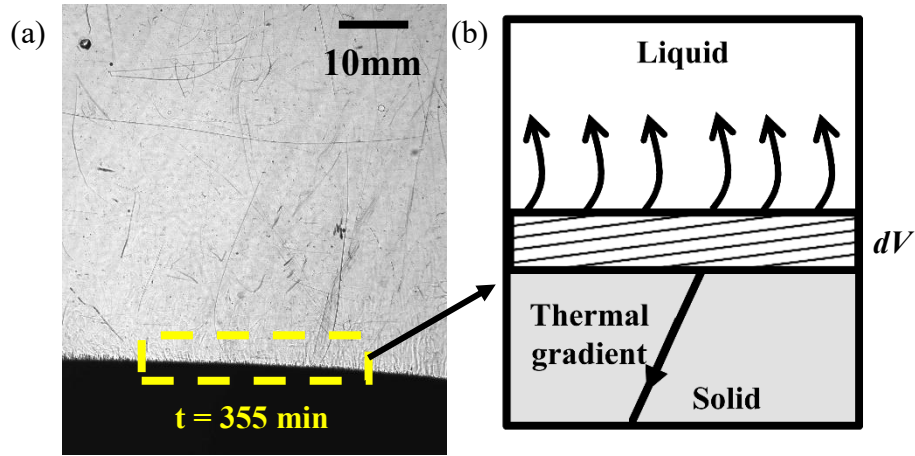


Figure 9: Energy balance at the liquid-solid interface in transition region (a) during faceted growth at 355min (b) schematic control volume.

It was assumed that the interface temperature of the growing solid was eutectic temperature, and the solid has uniform gradient. The gradient in the solid and the average solid-liquid interface position was taken at approximately 400 min (Figure 4(c)). In the presence of a negligible thermal gradient in the liquid due to random natural convection in the faceted case, a  $\Delta T_{change} = 13.1^\circ\text{C}$  can be estimated from Eq. (3), which is approximately equal to the experimental gain of temperature in the liquid (in the *transition regime*, Figure 6(a)). However, for the dendritic case wherein the thermal gradient in the liquid was approximately  $530^\circ\text{C/m}$ , the estimated  $\Delta T_{change}$  was approximately  $1.2^\circ\text{C}$  during a time interval of 1000-1400min.

After the reduction of local solutal convection, the composition ahead of the interface reached near eutectic. As the eutectic solid does not possess a mushy zone, a larger fraction of the solid was formed in the transition region compared to the previous regime. In the transition regime, a weak thermal gradient in the liquid was developed. The time scale for the development of the thermal

gradient in eutectic growth was  $\frac{\alpha}{V^2}$  ( $\sim 10^5$  sec), which is larger than the time duration associated with the transition regime (300-500min $\sim 10^4$  sec). This comparison validates the hypothesis that the gain of temperature in the liquid is primarily due to the reduced transport of heat in the solid.

The analysis finds that the uncharacteristic temperature rise during the solidification of Water-KNO<sub>3</sub> mixture can be attributed to the localized solid fraction and morphology, controlled by the natural convection patterns ahead of the mushy zone. Though a length-scale such as the primary spacing was offered by the faceted morphology, the absence of secondary arms as that of the dendritic case meant that the liquid flow was completely restricted in the mushy zone. This was further aided by a higher solid fraction and early eutectic growth. Therefore, the fluid mixtures that freeze with low mushy zone permeability can exhibit a significant temperature increase during freezing. This study reveals the underlying physical mechanism behind the apparent heating of the liquid, which was previously thought to be associated with the laboratory surroundings.

## Conclusions

The present experimental study investigated the influence of natural convection during faceted and dendritic growth using bottom cooled solidification of water-23 wt% KNO<sub>3</sub> and water-24 wt% NH<sub>4</sub>Cl respectively, which form faceted and dendritic structures in the mushy region. Real-time visualization of the flow field was presented with the help of shadowgraph and PIV techniques. The Rayleigh numbers in the bulk liquid and mushy zones were defined based on the respective volumetric length scales. The values of solutal Rayleigh number in the mushy zone ( $Ra_C$ ) are 68 and 231, and the bulk fluid Ra ( $Ra_{C\_Bulk}$ ) are  $9.1 \times 10^9$  and  $1.7 \times 10^9$  for water-23 wt% KNO<sub>3</sub> and water-24wt % NH<sub>4</sub>Cl respectively.  $Ra_{C\_P}$  for the faceted case was found to be lower than the critical value for the formation of plumes (115), and therefore, a vigorous random convection resulted in homogenization of the thermal and compositional fields in the liquid. This resulted in a negligible thermal gradient ahead of the interface, and shifted the liquid composition to the eutectic, in much lesser time compared to the dendritic case. Further, the eutectic solidification meant that a larger fraction of the solid formed, and the latent heat associated with the solidification resulted in a temperature rise of the liquid as the removal of the heat through the solid is limited in poorly conducting materials. In the dendritic growth case, the formation of plumes meant that the

gradients were considerable and therefore the liquid showed gradual cooling throughout the solidification.

The study highlights the importance of mushy zone permeability, and sheds new insights into the role of natural convection in changing the bulk-fluid temperatures, which were previously attributed to fluctuations in the surroundings.

### **Acknowledgment**

Authors gratefully acknowledge the financial support from the Department of Science and Technology (DST), India (Grant No. EMR/2015/001140).

### **References**

- [1] H.E. Huppert, M.G. Worster, *Flows involving phase change*, CRC Press, 2012. doi:10.1201/b14241.
- [2] C. Beckermann, J.P. Gu, W.J. Boettinger, Development of a freckle predictor via rayleigh number method for single-crystal nickel-base superalloy castings, *Metall. Mater. Trans. A*. 31 (2000) 2545–2557. doi:10.1007/s11661-000-0199-7.
- [3] N. Shevchenko, S. Boden, G. Gerbeth, S. Eckert, Chimney Formation in Solidifying Ga-25wt pct In Alloys Under the Influence of Thermosolutal Melt Convection, *Metall. Mater. Trans. a-Physical Metall. Mater. Sci.* 44A (2013) 3797–3808. doi:DOI 10.1007/s11661-013-1711-1.
- [4] S.M. Copley, A.F. Giamei, S.M. Johnson, M.F. Hornbecker, The origin of freckles in binary alloys, *Metall. Trans.* 1 (1970) 2193–2204. papers2://publication/uuid/C23132B5-AA63-4868-B2A9-2AC831AB15F5.
- [5] L. Yuan, P.D. Lee, A new mechanism for freckle initiation based on microstructural level simulation, *Acta Mater.* 60 (2012) 4917–4926. doi:10.1016/j.actamat.2012.04.043.
- [6] S. Karagadde, L. Yuan, N. Shevchenko, S. Eckert, P.D. Lee, 3-D microstructural model of freckle formation validated using in situ experiments, *Acta Mater.* 79 (2014) 168–180. doi:10.1016/j.actamat.2014.07.002.
- [7] M.G. Worster, Convection in mushy layers, *Annu. Rev. Fluid Mech.* 29 (1997) 91–122. doi:10.1146/annurev.fluid.29.1.91.
- [8] T.M. Pollock, S. Tin, Nickel-Based Superalloys for Advanced Turbine Engines: Chemistry, Microstructure and Properties, *J. Propuls. Power.* 22 (2006) 361–374. doi:10.2514/1.18239.
- [9] J.C. Ramirez, C. Beckermann, Evaluation of a rayleigh-number-based freckle criterion for Pb-Sn alloys and Ni-base superalloys, *Metall. Mater. Trans. A*. 34 (2003) 1525–1536. doi:10.1007/s11661-003-0264-0.
- [10] Porter D A;Easterling K E, *Phase Transformations in metals and alloys*, second edi, Springer-science Business Media,B.V., 1992.
- [11] H.E. Huppert, The fluid mechanics of solidification, *J. Fluid Mech.* 212 (1990) 209–240. doi:10.1017/S0022112090001938.
- [12] R.C. Kerr, A.W. Woods, H.E. Huppert, M.G. Worster, Solidification of an alloy cooled from above part 1. Equilibrium growth, *J. Fluid Mech.* 216 (1990) 323–342. doi:10.1017/S002211209000074X.

- [13] I. Karaca, E. Çadirli, H. Kaya, N. Maraşlı, Directional solidification of pure succinonitrile and succinonitrile- salol alloys, *Turkish J. Phys.* 25 (2001) 563–574.
- [14] C.F. Chen, J.S. Turner, Crystallization in a Double-Diffusive System, *J. Geophys. Res.* 85 (1980) 2573–2593.
- [15] R.C. Kerr, A.W. Woods, H.E. Huppert, M.G. Worster, Solidification of an alloy cooled from above part 2. Non-equilibrium interfacial kinetics, *J. Fluid Mech.* 217 (1990) 331–348. doi:10.1017/S002211209000074X.
- [16] R.C. Kerr, A.W. Woods, H.E. Huppert, M.G. Worster, Solidification of an alloy cooled from above. Part 3. Compositional stratification within the solid, *J. Fluid Mech.* 218 (1990) 337–354. doi:10.1017/S0022112090001021.
- [17] J.A. Dantzig, M. Rappaz, Analytical solutions for solidification, in: *Solidification*, EPFL Press, 1994: pp. 165–170.
- [18] L.J. Bloomfield, H.E. Huppert, Solidification and convection of a ternary solution cooled from the side, *J. Fluid Mech.* 489 (2003) 269–299. doi:10.1017/S0022112003005172.
- [19] F. Chen, Formation of double-diffusive layers in the directional solidification of binary solution, *J. Cryst. Growth.* 179 (1997) 277–286. doi:10.1016/S0022-0248(97)00098-5.
- [20] V. Kumar, A. Srivastava, S. Karagadde, Compositional dependency of double-diffusive layers during binary alloy solidification: Full-field measurements and quantification, *Phys. Fluids.* 30 (2018) 113603. doi:10.1063/1.5049135.
- [21] A.F. Thompson, H.E. Huppert, M.G. Worster, A. Aitta, Solidification and compositional convection of a ternary alloy, *J. Fluid Mech.* 497 (2003) 167–199. doi:10.1017/S002211200300661X.
- [22] C. Beckermann, C.Y. Wang, Equiaxed dendritic solidification with convection: Part III. Comparisons with NH<sub>4</sub>Cl-H<sub>2</sub>O experiments, *Metall. Mater. Trans. A.* 27 (1996) 2784–2795. doi:10.1007/BF02652371.
- [23] A. Aitta, H.E. Huppert, M.G. Worster, Diffusion-controlled solidification of a ternary melt from a cooled boundary, *J. Fluid Mech.* 432 (2000) 201–217.
- [24] D.G. Cherkasov, M.P. Smotrov, K.K. Il'in, Topological transformation of the phase diagram of the potassium nitrate-water-n-butoxyethanol ternary system, *Russ. J. Phys. Chem. A.* 84 (2010) 922–927. doi:10.1134/S0036024410060063.
- [25] K. Tanaka, Measurements of self-diffusion coefficients of water in pure water and in aqueous electrolyte solutions, *J. Chem. Soc., Faraday Trans. 1.* 71 (1975) 1127–1131. doi:10.1039/F19757101127.
- [26] P.R. Chakraborty, P. Dutta, Study of Freckles Formation During Directional Solidification Under the Influence of Single-Phase and Multiphase Convection, *J. Therm. Sci. Eng. Appl.* 5 (2013) 021004 (1-11). doi:10.1115/1.4023601.
- [27] V. Kumar, A. Srivastava, S. Karagadde, Real-time observations of density anomaly-driven convection and front instability during solidification of water, *J. Heat Transfer.* 140 (2018) 042503(1)-042503(12). doi:10.1115/1.4038420.
- [28] V. Kumar, M. Kumawat, A. Srivastava, S. Karagadde, Mechanism of flow reversal during solidification of an anomalous liquid, *Phys. Fluids.* 29 (2017) 123603(1)-123603(11). doi:10.1063/1.5005139.
- [29] V. Kumar, A. Srivastava, S. Karagadde, Do the intrusive probes alter the characteristic length-scales of natural convection?, *J. Flow Vis. Image Process.* 25 (2018) 207–228.

## Appendix

The observation of random convection patterns was further corroborated by performing experiments on a similar binary mixture that exhibits faceted morphology upon solidification. The faceted growth and random convection were observed during solidification of water-18 wt%  $\text{Na}_2\text{SO}_4$  as shown in Figure A1, which were similar to water-23 wt%  $\text{KNO}_3$ . The temperature measurements show the three regimes as similar to the water- $\text{KNO}_3$  case as shown in Figure A2.

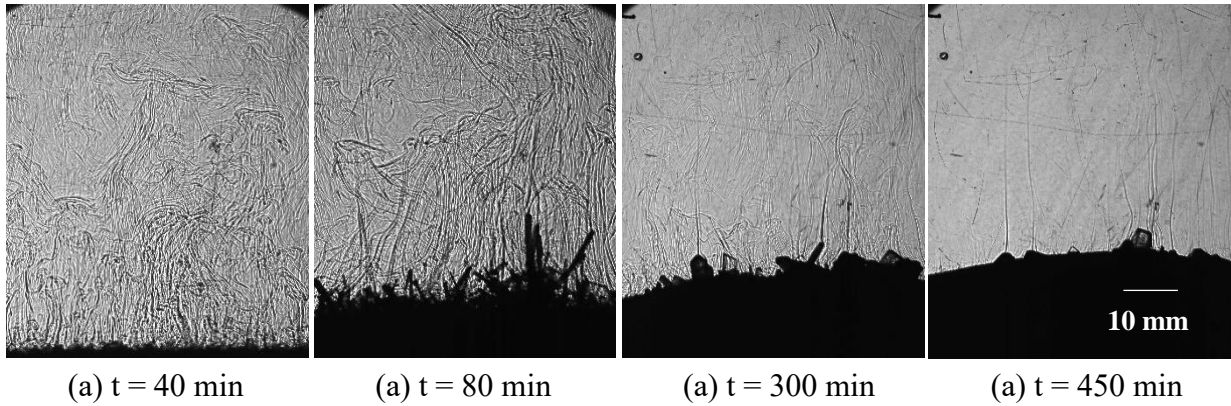


Figure A1: Convective flow observation using shadowgraph (a-d) for water-18 wt%  $\text{Na}_2\text{SO}_4$ : (a) random solutal convection at 60 min (b) similar flow at 260 min, and faceted microstructure was observed (c) reduction in convective strength (d) localized solutal convection and composition reached near eutectic composition and the sloped interface was observed at 450 min.

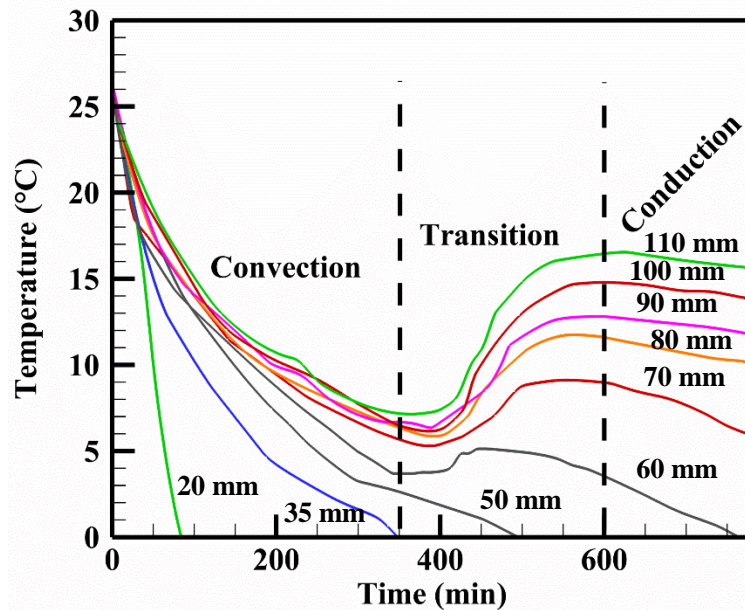


Figure A2: Temperature measurement at the different position in the cell during solidification of water-18 wt%  $\text{Na}_2\text{SO}_4$ .